

Microfluidic formulation of diazoxide-loaded solid lipid nanoparticles as a Novel approach for Friedreich's ataxia treatment

Ilaria Arduino^{a,1}, Antonella Santoro^{b,1}, Silvia De Santis^b, Rosa Maria Iacobazzi^a, Angela Assunta Lopodota^a, Eleonora Paradies^c, Giuseppe Merla^{d,e}, Sara Anjomani Virmouni^f, Luigi Palmieri^b, Carlo Marya Thomas Marobbio^{b,**}, Nunzio Denora^{a,*}

^a Department of Pharmacy – Pharmaceutical Sciences, University of Bari “Aldo Moro”, 70125, Bari, Italy

^b Department of Bioscience, Biotechnology and Environment, University of Bari, 70125, Bari, Italy

^c CNR Institute of Biomembranes, Bioenergetics and Molecular Biotechnologies (IBIOM), 70125, Bari, Italy

^d Department of Molecular Medicine & Medical Biotechnology, University of Naples Federico II, 80131, Naples, Italy

^e Laboratory of Regulatory & Functional Genomics, Fondazione IRCCS Casa Sollievo della Sofferenza, San Giovanni Rotondo, 71013, Foggia, Italy

^f Ataxia Research Group, Division of Biosciences, Department of Life Sciences, Brunel University London, Uxbridge, United Kingdom

ARTICLE INFO

Keywords:

Solid lipid nanoparticles
Microfluidics
Friedreich ataxia
Blood-brain barrier delivery

ABSTRACT

Friedreich ataxia (FRDA) is a hereditary autosomal recessive disorder characterized by frataxin deficiency, impacting mitochondrial function and causing oxidative damage. Diazoxide (DZX), a vasodilating drug used in the management of systemic hypertension, has shown promise in preclinical models but faces challenges in crossing the blood-brain barrier and potential toxicity at higher doses. This study aimed to create solid lipid nanoparticles (SLNs) loaded with DZX by microfluidic technique to improve blood-brain barrier (BBB) penetration and reduce side effects. Employing an *in vitro* BBB model, SLN-DZX demonstrated enhanced permeability compared to plain DZX. Cell viability assays carried out on FRDA fibroblast cells indicated enhanced viability with 1 μ M SLN-DZX. Cellular uptake studies confirmed SLN internalization in FRDA fibroblasts, and subsequent treatment with SLN-DZX significantly reduced both total and mitochondrial ROS levels compared to control and empty SLN-treated cells. These findings suggest SLN-DZX as a potential therapeutic approach for FRDA, mitigating oxidative stress with improved BBB penetration and reduced toxicity.

1. Introduction

Friedreich's ataxia (FRDA) (OMIM 229300) is a hereditary autosomal recessive disorder resulting from an increase in the GAA triplet repeat in the first intron of the FXN gene; on chromosome 9 [1]. In individuals without FRDA, the usual range of GAA repeats is typically between 5 and 30, while affected individuals exhibit a staggering 70 to over 1000 GAA trinucleotide expansions. This increase leads to a reduction in the transcription of FXN gene caused by heterochromatin establishment with or without epigenetic modifications [2] and its length correlates with the seriousness of FRDA clinical manifestations [3]. Although the precise role of FXN remains partially elusive, it is widely acknowledged to be implicated in regulation of cellular iron homeostasis. Oxidative injury, enzyme deficiencies and impaired

mitochondrial function are consequences of FXN insufficiency [4–6].

The primary pathological mechanism inherent neuropathy in FRDA consists of a progressive neurodegeneration resulting from the impairment of sensory neurons located in the dorsal root ganglia (DRG), a process that affects both the central and peripheral nervous systems [7, 8]. As the disease progresses, individuals with FRDA typically suffer a decline in motor coordination and muscle weakening, which occur 10–15 years after the disease first manifests and can result in a potential loss of motor function. Moreover, functional irregularities within the cardiovascular system are a significant feature of FRDA and can contribute to premature death, suggesting that cardiac complications are responsible for 60–80 % of premature deaths and means the leading factor to death of affected persons [7,8]. A pivotal milestone was achieved in 2023 with the United States Food and Drug Administration

* Corresponding author.

** Corresponding author.

E-mail addresses: carlomarya.marobbio@uniba.it (C.M.T. Marobbio), nunzio.denora@uniba.it (N. Denora).

¹ These authors contributed equally.

(FDA) approving omaveloxolone authorized as the first and sole treatment for FRDA in individuals who are at least 16 years of age (<https://www.fda.gov/drugs/news-events-human-drugs/fda-approves-first-treatment-friedreichs-ataxia>). However, it is important to note that while omaveloxolone represents a significant advancement as the first therapeutic agent targeting downstream events in FRDA, it does not provide a comprehensive remedy, particularly concerning the neurological aspects [9].

In 2018, we found that diazoxide (DZX) showed protective properties in FRDA cells and animal models by modulating the mTOR-S6K signaling pathway, promoting the translocation of NRF2 to the nucleus [10]. DZX, which is a derivative of benzothiadiazine, acts as a vasodilator employed in managing systemic hypertension, effectively reducing vascular resistance in the pulmonary circulation and allowing amelioration of symptoms in individuals affected by primary pulmonary hypertension [11]. DZX specifically interacts with the potassium-sensitive ATP channels located in the inner mitochondrial membrane (mitoKATP), which play pivotal roles in regulating mitochondrial respiration, altering mitochondrial membrane potential, and modulating mitochondrial matrix volume and reactive oxygen species (ROS) production to ensure neuronal survival [12–14].

Selective agonists of KATP channels have demonstrated their ability in protection from death caused by oxidative stress, inflammatory or excitotoxic insults in a wide range of cell types [15–17]. Although the potential therapeutic benefits of KATP channel agonists in preclinical models of neurodegenerative diseases, such as in a mouse model of Alzheimer's disease [18], in rat models of Parkinson's disease [19] and in animal models of multiple sclerosis [14,20], a phase 2 clinical trial, aimed to evaluate the efficacy of DZX, in patients with multiple sclerosis did not yield positive results [21]. This failure could be attributed to capability to penetrate the BBB and/or its bioavailability within the nervous system. Consequently, the efficacy of DZX for patients with neurological disorders warrants further investigation, as its ability to efficiently traverse the BBB remains a subject of debate. In addition, it is worth noting that DZX treatment may exhibit dose-dependent toxicity. Given that at elevated concentrations, DZX has the potential to inhibit succinate dehydrogenase activity, leading to an increase in ROS production [22]. YG8sr FRDA mouse model showed enhancements in fine motor coordination and balance after oral administration of 3 mg/kg DZX [10]. Additionally, the upregulation in the levels of both FXN and NRF2 mRNA expression and protein content in the heart and cerebellum following DZX administration led to reduced protein oxidation level and enhanced aconitase activity in liver, pancreas and brain [10,23]. However, this treatment exhibited adverse effects, such as a decline in overall locomotor activity. Notably, the concentration of 100 μ M DZX utilized in the treatment of human FRDA lymphoblastoid cells [10] corresponds approximately to the blood concentration of DZX in humans after 600 mg oral administration [24], representing the upper limit of the human dosage. In fact, to harness the full therapeutic potential of DZX for the treatment of FRDA, we aim to overcome potential limitations related to BBB permeability and bioavailability by encapsulating DZX within solid lipid nanoparticles (SLNs) [25]. Notably, the scientific literature has extensively shown SLNs' capacity to penetrate the BBB without the requirement for functionalization [26,27]. Our research efforts also utilized microfluidics to prepare DZX-loaded SLNs. This innovative technique enabled us to consistently produce nanosystems with a reduced size distribution and improved batch-to-batch reliability [28–32]. Specifically, our study investigates the ability of DZX-loaded SLNs i) to penetrate an *in vitro* transwell model, consisting of a monolayer of polarized endothelial cells, and ii) to enhance the functional and biochemical characteristics in a fibroblast cell line obtained from a patient affected by FRDA.

2. Materials and methods

2.1. Materials

No purification or distillation was performed; all chemicals were acquired at the highest possible purity and utilized exactly as received. Cetyl palmitate was provided by Farmalabor (Italy). Diazoxide, Lutrol F68 (Poloxamer 188), FITC-dextran 4000 (FD4), diazepam, 3-(4,5-Dimethylthiazolyl-2)-2,5-diphenyltetrazolium bromide (MTT) and double-distilled water were purchased from Sigma-Aldrich (Italy). Dihydrorhodamine 123 (DHR) and 2',7'-dichlorodihydrofluorescein diacetate (H2DCFDA) were from Life Technologies. Dulbecco's Modified Eagle Medium (DMEM), DMEM/F12 Medium, penicillin (100 U/mL) and streptomycin (100 μ g/mL), Fetal Bovine Serum (FBS) were from EuroClone. EndoGRO basal medium and medium supplements were from Merck. Culture flasks and Petri dishes were from Corning (Glassworks) and EuroClone.

2.2. Fibroblast and hCMEC/DE3 cell lines and culture conditions

FRDA fibroblasts were isolated from a patient carrying homozygous pathological alleles exhibiting 830/900 GAA repeat expansions. The healthy control and fibroblast cell lines from FRDA patient were cultured in DMEM/F12 medium supplemented with glutamine (2 mM), fetal bovine serum (10 %), penicillin (100 U/ml) and streptomycin (0.1 mg/ml). The cells were maintained at 37 °C in a humidified atmosphere with 5 % CO₂ in culture flasks. The pharmacological compound assays were carried out without antibiotics in the medium. Immortalized human cerebral microvascular endothelial (hCMEC/D3) cells were obtained from Pierre-Olivier Couraud at the Université Paris Descartes, Paris, France. The cells, maintained between passages 25 and 35, were cultured in EndoGRO media supplemented with the EndoGRO-MV supplement kit, basic fibroblast growth factor (200 ng/ml), penicillin-streptomycin (1 %), lithium chloride (10 mM), and resveratrol (10 M).

2.3. Preparation of DZX-loaded solid lipid nanoparticles

SLNs were synthesized via a nanoprecipitation technique employing a Fluidic 187 Herringbone mixer, a polycarbonate microfluidic device (Microfluidic Chip Shop, Jena Germany). The organic phase comprised cetyl palmitate in ethanol at a concentration of 10 mg/ml with 2 mg/mL of DZX, while the aqueous phase contained 2 % (w/v) Pluronic F68. The organic and aqueous phases served as the inner and outer fluids, respectively. Employing two microfluidic pumps, we regulated the flow rate of the inner (1 mL/min) and outer solution (5 mL/min), maintaining a constant flow rate. The fluids were directed from their respective syringes into the devices through minute tubes. Following synthesis, SLNs were meticulously purified to eliminate surfactant and non-encapsulated drug using centrifugal concentrators (Centrifugal Filter Units-Amicon Ultra 50 k) with ultrapure water at 4 °C, 3500 rpm for 15 min (repeated 5 times). Subsequently, the purified SLNs were stored at 4 °C. To assess cellular uptake of SLNs, BDP was incorporated into the organic phase at a ratio of 1/100 w/w of BDP/lipids.

2.4. Particle size, size distribution and surface charge

Characterization of the SLNs involved measuring size, polydispersity index (PDI), and zeta (ζ)-potential through dynamic light scattering utilizing a Malvern Zetasizer Nano instrument (Malvern Ltd., UK). Each sample, diluted 1:50 in double-distilled water, underwent analysis with approximately 1 mL using disposable polystyrene cuvettes (Sarstedt AG & Co., Germany) at 25 \pm 0.1 °C. The surface ζ -potential of the SLNs was assessed using a 750 μ L aliquot of the 1:50 dilution in demineralized water of the nanoparticle suspension within a disposable folder capillary cell (DTS1070, Malvern Instruments ltd., UK). These experiments were conducted in triplicate, and the resulting data are presented as the mean

numerical values alongside their standard deviations for each triplicate.

2.5. Transmission electron microscope imaging

For analysis of SLNs morphology and size distribution, a transmission electron microscope (TEM, Jeol JEM-1400, Jeol Ltd., Japan) was utilized. Specifically, a 10 μ L suspension of SLNs was deposited onto a carbon-coated copper grid (300 mesh; Electron Microscopy Sciences, USA) for 5 min. Subsequently, the samples were negatively stained with uranyl acetate by applying 2 μ L of a 2.1 % uranyl acetate solution onto the grids for approximately 2 min. Afterward, the grids underwent a single wash with 5 μ L of Milli-Q water for 5 min to eliminate excess uranyl acetate. Finally, the grids were left to air dry overnight before imaging.

2.6. Evaluation of drug encapsulation efficiency

The encapsulation efficiency (EE %) of DZX loaded within the hydrophobic core of SLNs was determined by measuring the drug content in 500 μ L of the SLNs aqueous dispersion. To solubilize the lipid matrix, SLNs were dissolved in 2 mL of hexane, while 2 mL of DMSO was employed for DZX extraction. The DZX content in DMSO was analyzed using UV–vis spectroscopy (PerkinElmer Lambda Bio20) by exploiting the absorbance peak at 272 nm. The concentration of DZX was determined using a calibration curve. The EE% of the drug was calculated using the following formula [33,34]:

$$\text{Encapsulation Efficacy (\%)} = \frac{\text{Weight of drug in SLN}}{\text{Weight of drug added initially}} \times 100$$

2.7. In vitro drug release studies

The Franz cells were utilized to perform DZX release assays from SLNs [35], with investigations specifically conducted under conditions both with and without human serum present in the donor compartment. In detail, 300 μ L of DZX-SLNs dispersion was diluted with 300 μ L of either water or human serum and applied onto an artificial cellulose acetate membrane (0.1–0.5 kDa, Fisher Scientific Milano), acting as a diffusion barrier (0.6 cm² area) between donor and receptor cells. Phosphate buffer (PBS, 10 mM, pH 7.4) served as the receptor medium, maintained at a constant temperature of (37 \pm 0.5) $^{\circ}$ C with continuous stirring. Over a duration of 96 h, 0.4 mL samples were withdrawn from the receiving compartment at predetermined intervals, and to ensure sink conditions, an equivalent volume of fresh PBS was replenished into the receptor cell. The collected samples were analyzed via UV/Vis spectroscopy to quantify the drug content. Each trial was conducted in triplicate across three independent Franz cells and with three distinct batches of SLNs.

2.8. In vitro model of BBB

hCMEC/DE3 cellular cultures (with a density of 50000 cells per square centimeter) were introduced onto the upper surface of transwell inserts (composed of polyester with 12 wells, featuring pores measuring 0.4 μ m, and translucent membrane inserts with a surface area of 1.12 square centimeters; Costar). These cultures were incubated for a duration of 14 days at a temperature of 37 $^{\circ}$ C, in an atmosphere containing 5 % CO₂, and under conditions of saturated humidity. This incubation period aimed to establish an in vitro representation of the BBB. Subsequently, at intervals of 2–3 days, the growth medium (500 mL in the upper compartment and 1 mL in the lower compartment) was refreshed. Utilizing an STX2 electrode epithelial volt-ohm meter (manufactured by World Precision Instruments, located in FL, USA), the transendothelial electrical resistance (TEER) across the cellular monolayer was gauged as an indicator of tight junction (TJ) formation progression.

2.9. Cell viability of DZX-SLN formulation

Evaluation of the viabilities of SLNs and DZX-SLNs on fibroblast and hCMEC/D3 cells were tested by MTT assay [36]. More precisely, cells were allocated into 96-well plates at a density of 66,000 cells per square centimeter and cultured with SLNs and DZX-SLNs dispersed in cellular medium at DZX concentrations of 75, 25, 10, 5, and 1 μ M, maintaining a temperature of 37 $^{\circ}$ C and 5 % CO₂. Following a 24-h incubation period, the medium was removed, and the wells were treated with 100 μ L of MTT solution (0.5 mg/mL in cell culture medium) and subsequently incubated at 37 $^{\circ}$ C. After 2 h, the absorbance at 570 nm was measured using a spectrometer (SPECTROstar Nano, BMG Labtech). The untreated cells served as the control. This assay relies on the mitochondrial activity of viable cells to convert water-soluble MTT into water-insoluble formazan crystals, a process facilitated by the mitochondria's reductive activity. The methodology employed in this assay mirrors descriptions provided elsewhere [10,36,37].

2.10. Endothelial permeability of DZX-SLN across the in vitro BBB model

On the 14th day of hCMEC/D3 cultivation within the transwell setup, DZX-SLN (with a DZX concentration of 1 μ M) suspended in PBS was introduced into the apical compartment of the transwell. Following a 3-h interval, samples were collected from the basolateral compartments, and the DZX concentration was determined utilizing UV–vis spectroscopy. The potential impact of SLNs on the integrity of the cellular monolayer was assessed by estimating the paracellular permeability of FITC-dextran 4000 (FD4) and the transcellular permeability of diazepam. In summary, 500 μ L of FD4 (200 μ g/mL in PBS) and diazepam (75 μ M in PBS) were administered into the apical compartment of the transwell system and allowed to incubate for up to 3 h at 37 $^{\circ}$ C. Calibration curves had been previously established by correlating fluorescence intensity values with the concentration of standard solutions for FD4. FD4 samples underwent analysis using a Victor3 fluorimeter (Wallac Victor3, 1420 Multilabel Counter, PerkinElmer) at excitation and emission wavelengths of 485 nm and 535 nm, respectively. Diazepam was detected via UV–vis spectroscopy, leveraging the absorbance peak at 230 nm. The endothelial permeability (EP) of the SLNs formulation, FD4, and diazepam were computed as previously outlined [27].

2.11. In vitro SLNs uptake

The internalization of the DZX-SLNs was investigated in vitro in fibroblasts from FRDA patient by means of fluorescence imaging. For these experiments, cells were seeded on glass coverslips (3x10⁴ cells/coverslip) and allowed to attach for 24 h (60 % confluence). Subsequently, the cells were treated with BODIPY (BDP)-loaded SLNs, after being incubated for 30 min at 4 $^{\circ}$ C, and then analyzed at specific time points using a Zeiss Axiovert 200 inverted epifluorescence microscope using a 63x/1.30 Ph3 oil objective and filter sets for BDP acquisition. The acquired images were captured using a CoolSNAP HQ CCD camera manufactured by Roper Scientific (Trenton NJ, USA) and MetaFluor 6.1 software developed by Universal Imaging Corporation (Downington, PA, USA). μ m.

2.12. ROS analysis

In order to detect intracellular ROS, cells were treated with the fluorogenic dye H2DCFDA. Upon entering the cell, H2DCFDA, converted into a non-fluorescent compound by cellular esterases. Afterward, this compound is oxidized by ROS, resulting in the production of the fluorescent 2,7-dichlorofluorescein (DCF) [38].

Fibroblasts from FRDA patient were grown in 96-well plate and treated with DZX-SLN (DZX 1 μ M) and empty-SLN (equivalent concentration of lipid core) (37 $^{\circ}$ C, 5 % CO₂). The cells were treated for 24 h, followed by a washing step and subsequent incubation with H2DCFDA

in DMEM/F12 medium without supplemented serum. The evaluation of DCF fluorescence was performed by a microplate reader (Victor 3, PerkinElmer) (excitation/emission wavelengths 488/535 nm). Results were normalized using each sample protein concentration and expressed as Relative Fluorescence Unit (RFU).

Mitochondrial ROS production was assessed using the dye dihydro-rhodamine 123 (DHR) (Life Technologies). DHR is able to enter the mitochondria and emits fluorescence upon oxidation by ROS, primarily peroxynitrite, leading to the formation of the positively charged rhodamine 123 derivative [39,40]. In brief, cells from FRDA patients were seeded on a slide and treated with DZX-SLN and empty-SLN for 24 h. Subsequently, the cells were incubated with DHR in DMEM/F12 medium without supplemented serum. Cellular fluorescence was therefore captured using a Zeiss Axiovert 200 inverted epifluorescence microscope using a 63x/1.30 Ph3 oil objective and filter sets for DHR acquisition (excitation/emission at 488/510 nm).

2.13. Statistical analysis

The experimental results are presented as mean \pm SD (standard deviation). Statistical evaluations were carried out utilizing Graph Prism version 8.0.1 (GraphPad Software Inc., La Jolla, CA, USA). In assessing the statistical significance of data sets, Two-way ANOVA analysis was employed, followed by Bonferroni's post hoc tests, with a threshold of $p < 0.0001$. Statistically significant disparities are denoted as follows: ns = p value > 0.05 ; * = $p < 0.0332$; ** = p value < 0.0021 .

3. Results and discussion

3.1. Preparation and characterization of solid lipid nanoparticle-loaded DZX

DZX-loaded SLNs were manufactured in a single continuous step using a microfluidic device. The microfluidic method has gained significant traction in the realm of nanomedicine, showcasing its clear advantages over traditional methods in recent times. Based on existing literature [27–29,31], microfluidics stands out as a promising tool for generating secure, swift, exceptionally reproducible, and dependable drug delivery systems. Moreover, conventional SLNs production techniques utilize non-sustainable solvents, leading to much longer production times and reduced efficiency. Additionally, the significance of the microfluidic method lies in its capacity to scale up the fabrication process, bridging the gap between academic research and practical industrial application [41]. SLNs were manufactured by a nanoprecipitation process using a polycarbonate device with a specific internal geometry called "herringbone". The internal herringbone geometry provides passive mixing; in fact, the use of a special design of the device's internal channels breaks up the laminar flow by increasing the contact area between the two fluids and reducing the diffusion length, thereby improving fluid mixing, and allowing nanoparticles with sizes below 200 nm to be obtained. The device channels have a depth of 200 μ m while the width of the mixing channel is 600 μ m. In literature, there are many examples exploring the proficiency of the staggered herringbone structure to ensure the formation of nanosized monodisperse nanoformulations [42]. Consequently, the given geometry enables the generation of rotational flow conditions caused by the chaotic aversion phenomenon at intermediate Reynolds numbers. The direction of the flows within the microfluidic device is redirected multiple times under this condition, reducing the diffusion time of the molecules and enabling quicker production with a high degree of monodispersity and narrower size range [42].

The SLNs fabricated via microfluidics underwent comprehensive characterization, with findings detailed in Table 1. SLN-DZX exhibited an average size of 180.1 ± 3.2 nm and a PdI of 0.125 ± 0.020 , while empty SLNs displayed an average size of 175.3 ± 1.2 nm and a PdI of 0.129 ± 0.03 . SLNs demonstrated a narrow size distribution, as

Table 1

Intensity-average hydrodynamic diameter and corresponding PdI determined by DLS, ζ -potential value, drug encapsulation efficiency (EE, %) of empty SLNs and SLN-DZX.

Formulations	Empty SLNs	SLN-DZX
d_{mean} (nm)	175.3 ± 1.2	180.1 ± 3.2
Polidispersity index (PdI)	0.129 ± 0.030	0.125 ± 0.020
ζ - potential (mV)	-42.5 ± 3.2	-31.8 ± 0.1
Encapsulation Efficiency (EE%)	/	85.6 ± 10.2

indicated by their low PdI values. The ζ potential for bare SLNs was also found to be -42.5 ± 3.2 mV, consistent with SLN-DZX, which exhibited a ζ potential of -31.8 ± 0.1 mV. The Encapsulation Efficiency (EE %) values for SLN-DZX represent the percentage (w/w, %) of the drug incorporated into the lipid core of SLNs relative to the initial drug amount used in the preparation of lipid nanovectors. The satisfactory EE % value obtained was 40.4 ± 6.8 %, affirming the optimization of nanoparticle properties, including drug encapsulation efficiency, facilitated by the microfluidic-assisted preparation method.

The morphology of PEG-SLNs was subsequently examined through TEM analysis (Fig. 1). TEM imaging unveiled particle sizes consistent with those obtained via DLS, with no signs of particle aggregation or clustering observed.

The in vitro drug release investigation was carried out on SLN-DZX utilizing Franz diffusion cells at a temperature of 37 °C in PBS (pH 7.4). As indicated in previous research, drug release from lipid-based nanoparticles is attributed to the degradation of the lipid matrix by cellular enzymes [31]. Consequently, experiments were performed both with and without human serum in the donor compartment. It was evident that in the absence of human serum, there was no discernible release of DZX from the formulation (Fig. 2), whereas in the presence of human serum, the percentage of DZX released from the SLNs reached 97.3 % within 96 h of incubation. Moreover, as widely reported [27–29, 31,43] in the literature SLNs are highly stable drug delivery systems due to the presence of the lipid core, showing limited phenomena of aggregation and surfactant expansion over time when tested in PBS.

3.2. Permeability of SLN-DZX through the in vitro BBB cell models

To investigate the capacity of SLN-DZX to traverse the BBB, an in vitro transwell model was established. This model comprised a polarized monolayer of endothelial cells seeded onto a porous membrane, facilitating the formation of an apical compartment (representing the "blood" side) that was physically distinct from the basolateral compartment (representing the "brain" side) [27,44]. The monolayer of hCMEC/D3 is an adequate model able to mimic properly the BBB physiological condition as it keeps well-represented most of the receptors and transporters which are expressed in vivo, thus enabling the cellular and molecular research drug transport pathways with central nervous system relevance [27]. To control the viability of the in vitro model, TEER values were checked during the formation of hCMEC/D3 monolayer. TEER values increased from 134.2 ± 3.4 Ω (1 day after seeding) to 172.9 ± 2.7 Ω (on the day 15th after seeding).

Before evaluating the ability of SLNs to cross the BBB model in vitro, the MTT assay was employed to examine cell viability after treatment of hCMEC/D3 cells with SLNs and SLNs-DZX (Fig. 3A). Cell viability was evaluated 24 h following the administration of escalating concentrations of drug-loaded SLNs (with drug concentrations ranging from 1 to 75 μ M) to hCMEC/D3 cells.

The results indicated that none of the concentrations of the vehicle used exhibited toxicity. Conversely, at the highest concentration of DZX, SLNs-DZX exhibited a slightly enhanced toxic effect compared to the drug administered alone. In contrast, for other concentrations (25, 10, 5, and 1 μ M), when DZX was encapsulated within SLNs, it was observed to have no adverse impact on endothelial cells. Furthermore, the data

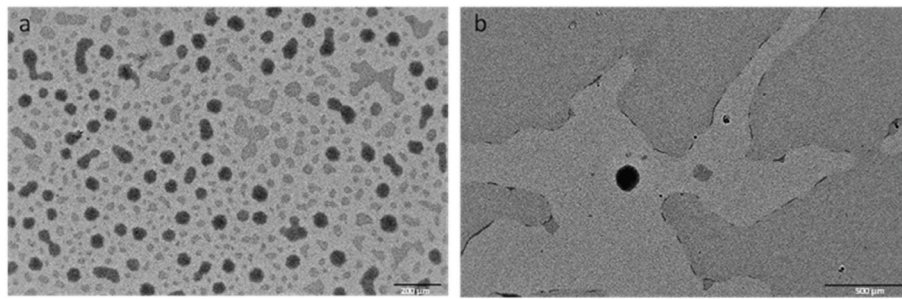


Fig. 1. a) Representative TEM micrograph obtained with staining for SLNs. b) Micrograph at higher magnification.

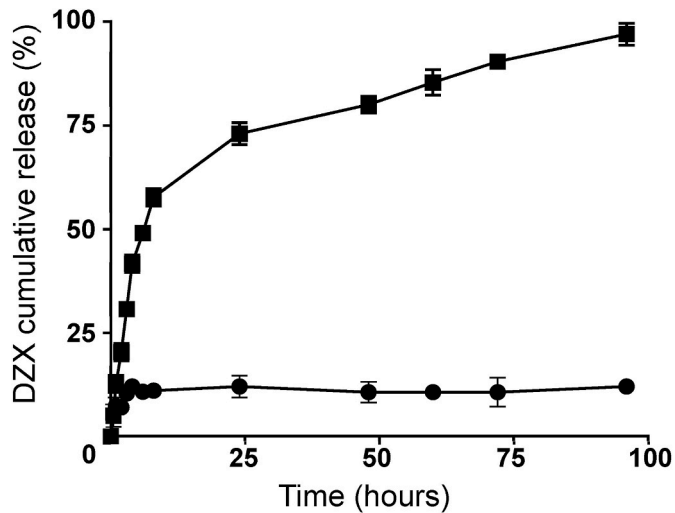


Fig. 2. In vitro release profiles of DZX from SLNs in PBS at 37 °C. SLNs were diluted with water (filled circles) or human serum (filled squares) in the donor compartment. Mean \pm SD are reported, n = 3.

revealed that at lower concentrations, DZX, when encapsulated within the SLNs, displayed a notably more pronounced increase in cell viability compared to untreated cells (see Fig. 3A).

The permeation across the monolayer of hCMEC/D3 was evaluated after 3 h of incubation by measuring the amount of DZX, Diazepam and FD4 collected in the basolateral compartment. The transport rates of Diazepam and FD4 were carried out in the absence and after treatment with the SLNs formulations, to evaluate the tight junction integrity, namely, to evaluate the transcellular permeability was used diazepam at final concentration of 75 μ M, while for the paracellular pathway was applied FD4 at 200 μ g/mL.

In particular, the permeation experiments through the hCMEC/D3 cell monolayer were carried out using identical concentrations of plain DZX and DZX encapsulated within SLNs, both set at 1 μ M. This formulation contained the lowest DZX concentration that exerted an increase of cell viability (Fig. 3A). The endothelial permeability (EP, P_{app}) values recorded with DZX and SLN-DZX were $9.3 \pm 1.2 \times 10^{-5}$ cm/s, and $12.2 \pm 0.6 \times 10^{-5}$ cm/s respectively (Table 2). Data resulting showed a slight increase in the P_{app} of the DZX encapsulated within SLNs in comparison with plain DZX. As reported in the literature [27,45] SLNs have proven to be valuable as nano drug delivery systems, taking into account the significant protection of the payload by the lipid core, which guards against rapid in vivo degradation. Moreover, applying a surfactant coating to the nanosystems introduces a steric hindrance, slowing down both the opsonization process and the swift clearance from the reticuloendothelial system (RES). The enhanced retention of SLNs in brain capillaries, along with their adherence to capillary walls, could result in an elevated concentration gradient. This, in turn, could enhance drug delivery to the brain by facilitating improved transport across the endothelial cell layer [46]. These favorable pharmacokinetic attributes enable SLNs to reach the target site unchanged, where internalization primarily occurs by exploiting the mechanism of clathrin-mediated endocytosis. Following uptake, the nanosystem may follow either the lysosomal or endosomal route. In the former case, the lipid matrix degrades, leading to the

Table 2

Permeation experiments through hCMEC/D3 cells monolayer were performed by using concentration of DZX loaded into SLNs of 1 μ M. The ability of SLNs to cross the in vitro BBB model was assessed at 3 h.

Compound	P_{app} AP cm/sec
DZX	$9.3 \pm 1.2 \times 10^{-5}$
SLN-DZX	$12.2 \pm 0.6 \times 10^{-5}$
Diazepam	$3.6 \pm 1.1 \times 10^{-5}$
FD4	$8.4 \pm 1.5 \times 10^{-5}$

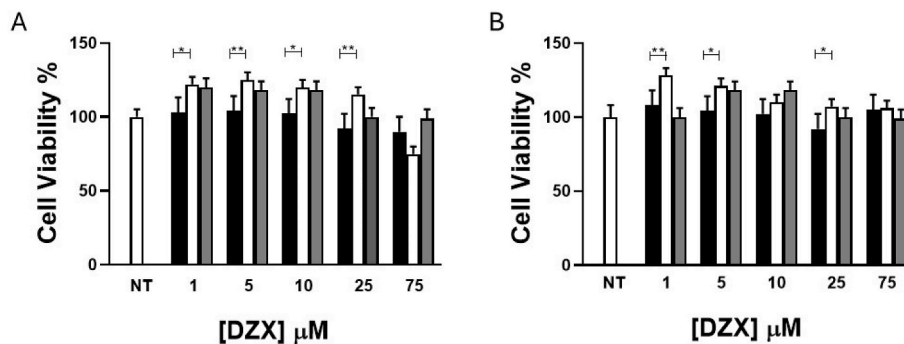


Fig. 3. (A) Cell viability of hCMEC/D3 after 24 h incubation with DZX (black bar), SLN-DZX (white bar) and SLNs (grey bar). (B) Cell viability of fibroblast cells of FRDA patient assessed after cells incubation DZX (black bar), SLN-DZX (white bar) and SLNs (grey bar) for 24 h. NT corresponds to untreated cells. Each compound was tested in triplicate, and the experiments were repeated three times. A difference was significant with * $p < 0.0332$ and ** $p < 0.0021$.

release of the drug into the cell, while the endosome transports the entire nanosystem to the opposite pole of the barrier, facilitating the release of the embedded drug in the brain compartment [45].

3.3. Cell viability of fibroblast cell lines treated with DZX, empty SLN or SLN-DZX

The cell viability study was assessed by MTT assay on fibroblast cell of FRDA patient by incubating them with various conditions, including exposure to DZX, SLN-DZX, and SLN for durations of 24 h (Fig. 3B). The results showed that DZX, whether in its free form or encapsulated within SLNs, did not exhibit any toxic effects. Additionally, the tested concentration range revealed that SLNs devoid of DZX were not cytotoxic. Interestingly, the 1 μ M DZX-SLN treatment led to a notably more significant improve in cell viability. Consequently, the treatment of choice was determined to be the use of 1 μ M DZX-SLN.

3.4. In vitro uptake study of SLN

SLN uptake in cell was assessed by measuring the fluorescent signal in FRDA fibroblasts. FRDA fibroblast cells internalized SLN-BDP after incubation with 28.7 nM of BDP, corresponding to 75 μ g/ml of lipid core of SLN. Cells were seeded and treated in accordance with the procedure outlined in the experimental section. Fluorescence was analyzed at the time indicated. Fig. 4 showed the fibroblast uptake of SLN-BDP over time. Intense red fluorescence of SLN could be seen inside the cells after 6 min, indicating that fibroblast recognized SLN as material to be internalized. In addition, cells displayed a uniform cytoplasmic red fluorescence signal, indicating an effective incorporation of SLN.

3.5. SLN-DZX treatment decrease oxidative cell damage in fibroblast from FRDA patient

The pathogenesis of FRDA is significantly impacted by an accumulation of free radicals and oxidative stress [47]. Iron overload and dysfunction in mitochondria, which are associated with the mutation in the FXN gene, are thought to be a consequence of ROS production [10, 48]. The use of two distinct ROS-sensitive fluorogenic probes, H2DCFDA for cytosolic ROS and DHR123 for mitochondrial ROS, allowed the detection of oxidative stress within these specific cellular compartments [49,50].

Initially, we examined fibroblast cell lines derived from FRDA

patients, by a time-course analysis of fluorescence emission. This analysis aimed to quantify the overall levels of cellular ROS detected by H2DCFDA, a probe that can penetrate biological membranes despite being non-fluorescent. Once inside the cytosol, the probe becomes impermeable due to esterase activity, which converts it into 2',7'-dichlorodihydrofluorescein. ROS, primarily hydrogen peroxide (H_2O_2), then oxidize this compound, resulting in the formation of the fluorescent compound dichlorofluorescein (DCF). Fig. 5A demonstrates that FRDA patient showed higher level of cytosolic ROS production when compared to healthy control fibroblast cell line. Thus, to investigate whether the effect of DZX on FRDA fibroblasts involved the activation of antioxidant pathways, we analyzed ROS production after 24 h of SLN-DZX treatment. In the FRDA fibroblast treated with 1 μ M SLN-DZX, ROS level was decreased as compared with empty-SLN treatment (Fig. 5B).

Several studies conducted using cellular and animal models have consistently demonstrated that FXN insufficiency leads to a marked increase in ROS levels within the mitochondria, often linked to the increase of redox-active iron into this compartment [51–53].

In order to gain deeper insights into the impact of SLN-DZX on FRDA fibroblasts, we investigated the mitochondrial ROS production using fluorescence microscopy. This analysis involved the incubation of cells with the fluorescent probe DHR, which localizes within the mitochondria and emits fluorescence upon oxidation by ROS [39,40]. As shown in Fig. 6, a 24-h treatment with 1 μ M SLN-DZX resulted in a notable decrease in the fluorescence linked to mitochondrial ROS in FRDA fibroblasts, when compared to both the empty-SLN (eSLN) treatment and the untreated sample (NT).

Consequently, these findings strongly indicate that the SLNs have the capability to release the encapsulated DZX into the cells, leading to its antioxidant effects on both total and mitochondrial ROS.

4. Conclusions

Previous studies have unequivocally demonstrated the neuro-protective attributes of DZX in mitigating oxidative stress within cellular and animal models relevant to neurodegenerative and inflammatory pathologies, nevertheless it is noteworthy that an oral clinical trial involving DZX failed to yield the anticipated outcomes, probably due to the incapability of DZX to penetrate BBB. Considering this, our investigation sought to assess the permeability of unbound DZX across BBB cellular models. Our results indicate that DZX is able to cross these

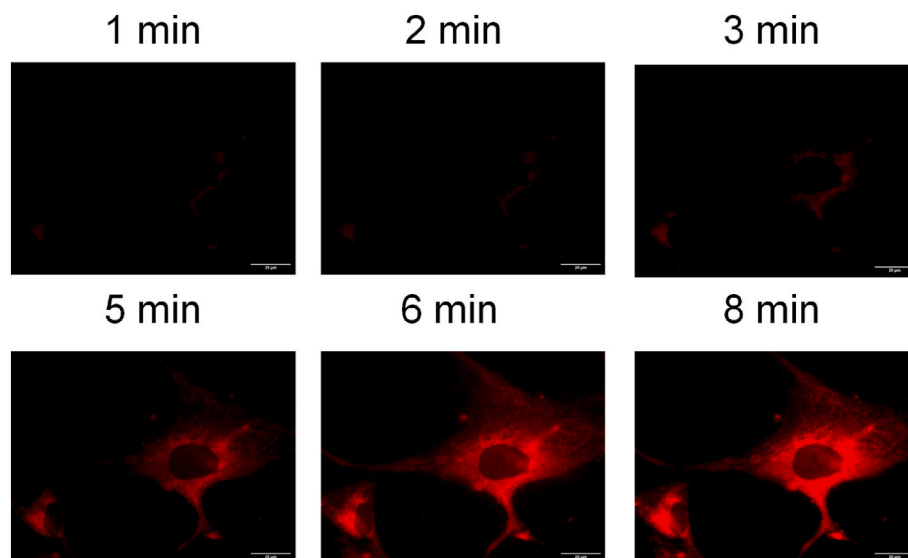


Fig. 4. Uptake of SLN-BDP in fibroblast assessed by fluorescence microscope. Cells were seeded on a microscopy slide. Fluorescence images were taken over time as fibroblast internalized SLN-BDP. BDP concentration was 28.7 nM equivalent to 75 μ g/mL of lipid core of SLN. Scale bar 20 μ m.

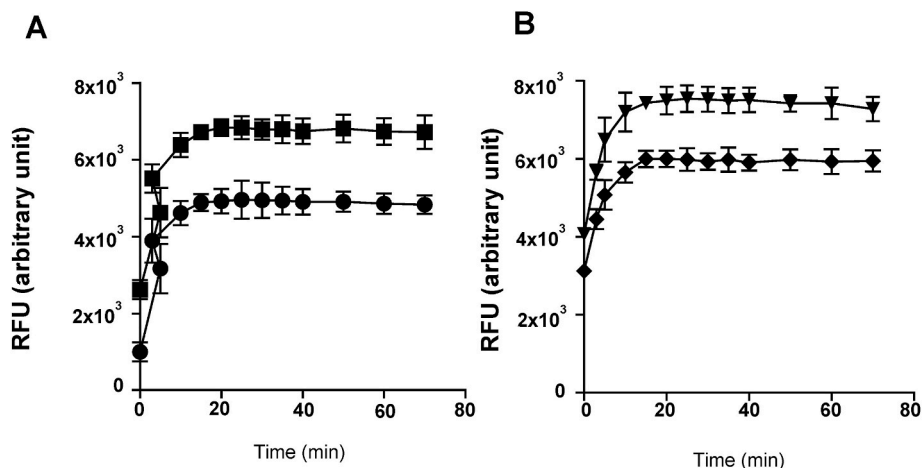


Fig. 5. Effect of SLN-DZX on ROS production in FRDA fibroblast. A) Time course of ROS production in fibroblasts assessed by DCF fluorescence. Fibroblast from healthy control (circle) and from FRDA patient (square) were maintained in complete DMEM/F12 medium and incubated with H2DCFDA (5 μ M) in a 5 % CO₂ incubator at 37 °C for 30 min. B) Time related changes of ROS level in fibroblast from FRDA patient after 24 h-treatment with empty-SLN (triangle) and DZX-SLN (diamond). Cells were maintained as described above and treated with SLNs. After 24 h treatment, cells were washed and incubated with H2DCFDA (5 μ M) in a 5 % CO₂ incubator at 37 °C for 30 min. ROS level was measured with a microplate reader (excitation/emission wavelengths 488/535 nm). Results are expressed as Relative Fluorescence Unit (RFU). Values represent mean \pm S. D, n = 3.

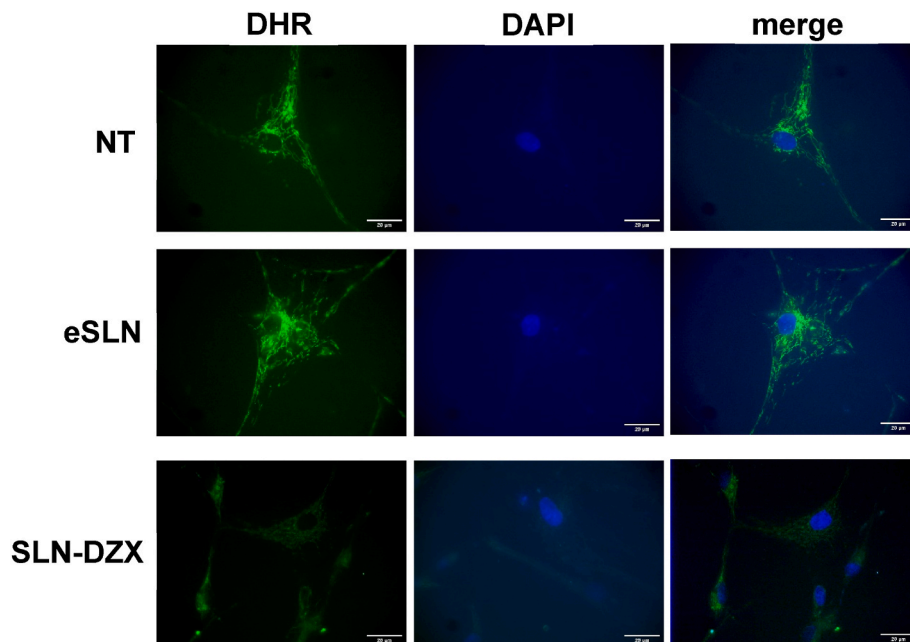


Fig. 6. Fluorescence microscopy of FRDA fibroblasts. Cells were seeded on a microscopy slide. After 24 h treatment with SLNs were washed twice with PBS and incubated with DHR (5 μ M) for ROS detection and DAPI (1 μ g/ml) for nuclei staining. NT, not treated. eSLN, empty SLNs. Scale bar 20 μ m.

barriers, but to potentially improve the bioavailability of DZX, we exploited the strategy of encapsulating DZX within SLN. This groundbreaking method has been pivotal in confirming the capability of the DZX-loaded formulation to cross BBB cellular models, exhibiting a slightly higher degree in comparison to the unencapsulated DZX. Additionally, it is noteworthy that the lipid core of SLN provides substantial protection to the payload, safeguarding against rapid in vivo degradation. We showed that the 1 μ M SLN-DZX formulation effectively releases the drug into frataxin-deficient fibroblasts, resulting in a discernible reduction in mitochondrial ROS production. In summary, our research underscores the efficacy of treatment with SLN-DZX as a potent pharmacological tool for modulating ROS production and metabolic activities. The collective evidence from this investigation offers a compelling case for considering SLN-DZX as a promising and

innovative formulation for safeguarding against oxidative stress induced damage and functional impairments in the context of FRDA.

CRedit authorship contribution statement

Iliaria Arduino: Writing – review & editing, Writing – original draft, Project administration, Methodology. **Antonella Santoro:** Writing – original draft, Methodology, Investigation. **Silvia De Santis:** Resources, Investigation. **Rosa Maria Iacobazzi:** Resources, Investigation. **Angela Assunta Lopodota:** Formal analysis, Data curation. **Eleonora Paradies:** Investigation, Data curation. **Giuseppe Merla:** Investigation, Data curation. **Sara Anjomani Virmouni:** Resources, Investigation. **Luigi Palmieri:** Investigation, Data curation. **Carlo Marya Thomas Marobbio:** Writing – review & editing, Data curation. **Nunzio Denora:**

Writing – review & editing, Supervision, Project administration.

Declaration of competing interest

The authors declare that they have no known competing financial interests or personal relationships that could have appeared to influence the work reported in this paper.

Data availability

Data will be made available on request.

Acknowledgments

We thank M.U.R.—Programma Operativo Nazionale (PON) “Ricerca e Innovazione” 2014–2020 Tematica IV.4 “Dottorati e Contratti di ricerca su tematiche dell’innovazione”.

References

- V. Campuzano, L. Montermini, M.D. Moltò, L. Pianese, M. Cossée, F. Cavalcanti, E. Monros, F. Rodius, F. Duclos, A. Monticelli, F. Zara, J. Canizares, H. Koutnikova, S.I. Bidichandani, C. Gellera, A. Brice, P. Trouillas, G. De Michele, A. Filla, R. De Frutos, F. Palau, P.I. Patel, S. Di Donato, J.-L. Mandel, S. Cocozza, M. Koenig, M. Pandolfo, Friedreich's ataxia: autosomal recessive disease caused by an intronic GAA triplet repeat expansion, *Science* 271 (1996) 1423–1427, <https://doi.org/10.1126/science.271.5254.1423>.
- J.M. Gottesfeld, Molecular mechanisms and therapeutics for the GAA-TTC expansion disease Friedreich ataxia, *Neurotherapeutics* 16 (2019) 1032–1049, <https://doi.org/10.1007/s13311-019-00764-x>.
- A. Filla, G. De Michele, F. Cavalcanti, L. Pianese, A. Monticelli, G. Campanella, S. Cocozza, The relationship between trinucleotide (GAA) repeat length and clinical features in Friedreich ataxia, *Am. J. Hum. Genet.* 59 (1996) 554–560.
- M. Pandolfo, Iron and Friedreich ataxia, in: *Parkinson's Disease and Related Disorders*, Springer Vienna, Vienna, 2006, pp. 143–146, https://doi.org/10.1007/978-3-211-45295-0_22.
- C. Lu, G. Cortopassi, Frataxin knockdown causes loss of cytoplasmic iron–sulfur cluster functions, redox alterations and induction of heme transcripts, *Arch. Biochem. Biophys.* 457 (2007) 111–122, <https://doi.org/10.1016/j.abb.2006.09.010>.
- A. Dürr, M. Cossee, Y. Agid, V. Campuzano, C. Mignard, C. Penet, J.-L. Mandel, A. Brice, M. Koenig, Clinical and Genetic Abnormalities in patients with Friedreich's ataxia, *N. Engl. J. Med.* 335 (1996) 1169–1175, <https://doi.org/10.1056/NEJM199610173351601>.
- M. Perdomini, B. Belbellaa, L. Monassier, L. Reutenauer, N. Messaddeq, N. Cartier, R.G. Crystal, P. Aubourg, H. Puccio, Prevention and reversal of severe mitochondrial cardiomyopathy by gene therapy in a mouse model of Friedreich's ataxia, *Nat. Med.* 20 (2014) 542–547, <https://doi.org/10.1038/nm.3510>.
- F. Weidemann, S. Störk, D. Liu, K. Hu, S. Herrmann, G. Ertl, M. Niemann, Cardiomyopathy of Friedreich ataxia, *J. Neurochem.* 126 (2013) 88–93, <https://doi.org/10.1111/jnc.12217>.
- V. Profeta, K. McIntyre, M. Wells, C. Park, D.R. Lynch, Omaveloxolone: an activator of Nrf2 for the treatment of Friedreich ataxia, *Expert Opin. Invest. Drugs* 32 (2023) 5–16, <https://doi.org/10.1080/13543784.2023.2173063>.
- A. Santoro, S. Anjomani Virmouni, E. Paradies, V.L. Villalobos Coa, S. Al-Mahdawi, M. Khoo, V. Porcelli, A. Vozza, M. Perrone, N. Denora, F. Taroni, G. Merla, L. Palmieri, M.A. Pook, C.M.T. Marobbio, Effect of diazoxide on Friedreich ataxia models, *Hum. Mol. Genet.* 27 (2018) 992–1001, <https://doi.org/10.1093/hmg/ddy016>.
- V. Campese, R. Lakdawala, The challenges of blood Pressure control in Dialysis patients, recent Advances in cardiovascular drug Discovery, Formerly Recent Patents Cardiovascul. Drug Discov. 10 (2016) 34–59, <https://doi.org/10.2174/1574890110666151116144725>.
- S. Arnon, E. Lagerev, J. Herzlich, A. Eliakim, I. Litmanovitz, Diazoxide treatment for persistent hypoglycemia in a small for gestational age preterm infant with adequate low insulin levels, *Case Rep. Perinat. Med.* 3 (2014) 83–85, <https://doi.org/10.1515/crpm-2013-0024>.
- M. Gómez-Barroso, K.M. Moreno-Calderón, E. Sánchez-Duarte, C. Cortés-Rojo, A. Saavedra-Molina, A.R. Rodríguez-Orozco, R. Montoya-Pérez, Diazoxide and Exercise enhance muscle Contraction during Obesity by decreasing ROS levels, lipid Peroxidation, and improving Glutathione redox Status, *Antioxidants* 9 (2020) 1232, <https://doi.org/10.3390/antiox9121232>.
- N. Virgili, J.F. Espinosa-Parrilla, P. Mancera, A. Pastén-Zamorano, J. Gimeno-Bayon, M.J. Rodríguez, N. Mahy, M. Pugliese, Oral administration of the KATP channel opener diazoxide ameliorates disease progression in a murine model of multiple sclerosis, *J. Neuroinflammation* 8 (2011) 149, <https://doi.org/10.1186/1742-2094-8-149>.
- K. Nagy, B. Kis, N.C. Rajapakse, F. Bari, D.W. Busija, Diazoxide preconditioning protects against neuronal cell death by attenuation of oxidative stress upon glutamate stimulation, *J. Neurosci. Res.* 76 (2004) 697–704, <https://doi.org/10.1002/jnr.20120>.
- E.M. Choi, G.-H. Kim, Y.S. Lee, Diazoxide protects against hydrogen peroxide-induced toxicity in the osteoblastic MC3T3-E1 cells, *Eur. J. Pharmacol.* 624 (2009) 45–50, <https://doi.org/10.1016/j.ejphar.2009.09.041>.
- M. Fornazari, J.G. de Paula, R.F. Castilho, A.J. Kowaltowski, Redox properties of the adenosine triphosphate-sensitive K⁺ channel in brain mitochondria, *J. Neurosci. Res.* 86 (2008) 1548–1556, <https://doi.org/10.1002/jnr.21614>.
- D. Liu, M. Pitta, J.-H. Lee, B. Ray, D.K. Lahiri, K. Furukawa, M. Mughal, H. Jiang, J. Villarreal, R.G. Cutler, N.H. Greig, M.P. Mattson, The KATP channel activator diazoxide ameliorates amyloid- β and Tau pathologies and improves memory in the 3xTgAD mouse model of Alzheimer's disease, *J. Alzheim. Dis.* 22 (2010) 443–457, <https://doi.org/10.3233/JAD-2010-101017>.
- Y. Yang, X. Liu, Y. Long, F. Wang, J.-H. Ding, S.-Y. Liu, Y.-H. Sun, H.-H. Yao, H. Wang, J. Wu, G. Hu, Activation of mitochondrial ATP-sensitive potassium channels improves rotenone-related motor and neurochemical alterations in rats, *Int. J. Neuropsychopharmacol.* 9 (2005) 51, <https://doi.org/10.1017/S1461145705005547>.
- N. Virgili, P. Mancera, B. Wappenhans, G. Sorrosal, K. Biber, M. Pugliese, J. F. Espinosa-Parrilla, KATP channel opener diazoxide Prevents neurodegeneration: a New mechanism of action via Antioxidative pathway activation, *PLoS One* 8 (2013) e75189, <https://doi.org/10.1371/journal.pone.0075189>.
- P. Villoslada, A. Rovira, X. Montalban, R. Arroyo, F. Paul, V. Meca-Lallana, C. Ramo, O. Fernandez, A. Saiz, A. Garcia-Merino, L. Ramió-Torrentà, B. Casanova, C. Oreja-Guevara, D. Muñoz, J.E. Martínez-Rodríguez, E. Lensch, J.M. Prieto, S. G. Meuth, X. Nuñez, C. Campás, M. Pugliese, Effects of diazoxide in multiple sclerosis, *Neurol. Neuroimmunol. Neuroinflamm.* 2 (2015), <https://doi.org/10.1212/NXI.0000000000000147>.
- D.W. Busija, P. Katakam, N.C. Rajapakse, B. Kis, G. Grover, F. Domoki, F. Bari, Effects of ATP-sensitive potassium channel activators diazoxide and BMS-191095 on membrane potential and reactive oxygen species production in isolated piglet mitochondria, *Brain Res. Bull.* 66 (2005) 85–90, <https://doi.org/10.1016/j.brainresbull.2005.03.022>.
- S.Y. Lew, M.W.L. Phang, P.S. Chong, J. Roy, C.H. Poon, W.S. Yu, L.W. Lim, K. H. Wong, Discovery of therapeutics targeting oxidative stress in autosomal recessive cerebellar ataxia: a Systematic review, *Pharmaceuticals* 15 (2022) 764, <https://doi.org/10.3390/ph15060764>.
- B. Calesnick, B. Katchen, J. Black, Importance of Dissolution rates in producing effective diazoxide blood levels in man, *J. Pharmaceut. Sci.* 54 (1965) 1277–1280, <https://doi.org/10.1002/jps.2600540911>.
- R.M. Iacobazzi, F. Vischio, I. Arduino, F. Canepa, V. Laquintana, M. Notarnicola, M.P. Scavo, G. Bianco, E. Fanizza, A.A. Lopodota, A. Cutrignelli, A. Lopalco, A. Azzariti, M.L. Curri, M. Franco, G. Giannelli, B.C. Lee, N. Depalo, N. Denora, Magnetic implants in vivo guiding sorafenib liver delivery by superparamagnetic solid lipid nanoparticles, *J. Colloid Interface Sci.* 608 (2022) 239–254, <https://doi.org/10.1016/j.jcis.2021.09.174>.
- F. Sommonte, I. Arduino, G.F. Racaniello, A. Lopalco, A.A. Lopodota, N. Denora, The Complexity of the blood-brain barrier and the Concept of age-related brain targeting: challenges and potential of Novel solid lipid-based formulations, *J. Pharmaceut. Sci.* 111 (2022) 577–592, <https://doi.org/10.1016/j.xphs.2021.08.029>.
- I. Arduino, N. Depalo, F. Re, R. Dal Magro, A. Panniello, N. Margiotta, E. Fanizza, A. Lopalco, V. Laquintana, A. Cutrignelli, A.A. Lopodota, M. Franco, N. Denora, PEGylated solid lipid nanoparticles for brain delivery of lipophilic kateplatin Pt(IV) prodrugs: an in vitro study, *Int. J. Pharm.* 583 (2020) 119351, <https://doi.org/10.1016/j.ijpharm.2020.119351>.
- I. Arduino, Z. Liu, R.M. Iacobazzi, A.A. Lopodota, A. Lopalco, A. Cutrignelli, V. Laquintana, L. Porcelli, A. Azzariti, M. Franco, H.A. Santos, N. Denora, Microfluidic preparation and in vitro evaluation of iRGD-functionalized solid lipid nanoparticles for targeted delivery of paclitaxel to tumor cells, *Int. J. Pharm.* 610 (2021) 121246, <https://doi.org/10.1016/j.ijpharm.2021.121246>.
- I. Arduino, Z. Liu, A. Rahikkala, P. Figueiredo, A. Correia, A. Cutrignelli, N. Denora, H.A. Santos, Preparation of cetyl palmitate-based PEGylated solid lipid nanoparticles by microfluidic technique, *Acta Biomater.* 121 (2021) 566–578, <https://doi.org/10.1016/j.actbio.2020.12.024>.
- R.M. Iacobazzi, I. Arduino, R. Di Fonte, A.A. Lopodota, S. Serrati, G. Racaniello, V. Bruno, V. Laquintana, B.-C. Lee, N. Silvestris, F. Leonetti, N. Denora, L. Porcelli, A. Azzariti, Microfluidic-assisted preparation of targeted pH-Responsive Polymeric Micelles improves Gemcitabine Effectiveness in PDAC: in vitro insights, *Cancers* 14 (2021) 5, <https://doi.org/10.3390/cancers14010005>.
- F. Sommonte, I. Arduino, R.M. Iacobazzi, M. Tiboni, F. Catalano, R. Marotta, M. Di Francesco, L. Casertari, P. Decuzzi, A.A. Lopodota, N. Denora, Microfluidic assembly of “Turtle-Like” shaped solid lipid nanoparticles for lysozyme delivery, *Int. J. Pharm.* 631 (2023) 122479, <https://doi.org/10.1016/j.ijpharm.2022.122479>.
- I. Arduino, R. Di Fonte, M. Tiboni, L. Porcelli, S. Serrati, D. Fondaj, T. Rafaschieri, A. Cutrignelli, G. Guida, L. Casertari, A. Azzariti, A.A. Lopodota, N. Denora, R. M. Iacobazzi, Microfluidic development and biological evaluation of targeted therapy-loaded biomimetic nano system to improve the metastatic melanoma treatment, *Int. J. Pharm.* 650 (2024) 123697, <https://doi.org/10.1016/j.ijpharm.2023.123697>.
- P. Knoll, G. Francesco Racaniello, V. Laquintana, F. Veider, A. Saleh, A. Seybold, N. Denora, A. Bernkop-Schnürch, Lipid-based nanoparticles: enhanced cellular uptake via surface thiolation, *Int. J. Pharm.* 635 (2023) 122753, <https://doi.org/10.1016/j.ijpharm.2023.122753>.

- [34] T. Latronico, F. Rizzi, A. Panniello, V. Laquintana, I. Arduino, N. Denora, E. Fanizza, S. Milella, C.M. Mastroianni, M. Striccoli, M.L. Curri, G.M. Liuzzi, N. Depalo, Luminescent PLGA nanoparticles for delivery of Darunavir to the brain and inhibition of matrix Metalloproteinase-9, a relevant therapeutic target of HIV-associated neurological disorders, *ACS Chem. Neurosci.* 12 (2021) 4286–4301, <https://doi.org/10.1021/acscchemneuro.1c00436>.
- [35] A. Lopodota, A. Cutrignelli, V. Laquintana, N. Denora, R.M. Iacobazzi, M. Perrone, E. Fanizza, M. Mastrodonato, D. Mentino, A. Lopalco, N. Depalo, M. Franco, Spray Dried Chitosan Microparticles for Intravesical delivery of Celecoxib: preparation and characterization, *Pharm. Res. (N. Y.)* 33 (2016) 2195–2208, <https://doi.org/10.1007/s11095-016-1956-7>.
- [36] N. Depalo, M. Corricelli, I. De Paola, G. Valente, R.M. Iacobazzi, E. Altamura, D. Debellis, D. Comegna, E. Fanizza, N. Denora, V. Laquintana, F. Mavelli, M. Striccoli, M. Saviano, A. Agostiano, A. Del Gatto, L. Zaccaro, M.L. Curri, NIR Emitting Nanoprobes based on Cyclic RGD Motif Conjugated PbS Quantum Dots for Integrin-targeted Optical Bioimaging, *ACS Appl. Mater. Interfaces* 9 (2017) 43113–43126, <https://doi.org/10.1021/acscami.7b14155>.
- [37] V. Laquintana, N. Denora, A. Lopalco, A. Lopodota, A. Cutrignelli, F.M. Lasorsa, G. Agostino, M. Franco, Translocator protein Ligand–PLGA Conjugated nanoparticles for 5-Fluorouracil delivery to Glioma Cancer cells, *Mol. Pharm.* 11 (2014) 859–871, <https://doi.org/10.1021/mp400536z>.
- [38] A. Gomes, E. Fernandes, J.L.F.C. Lima, Fluorescence probes used for detection of reactive oxygen species, *J. Biochem. Biophys. Methods* 65 (2005) 45–80, <https://doi.org/10.1016/j.jbbm.2005.10.003>.
- [39] N. Kooy, J. Royall, H. Ischiropoulos, J. Beckman, Peroxynitrite-mediated oxidation of dihydrorhodamine 123, *Free Radic. Biol. Med.* 16 (1994) 149–156, [https://doi.org/10.1016/0891-5849\(94\)90138-4](https://doi.org/10.1016/0891-5849(94)90138-4).
- [40] M.P. Mattson, Y. Goodman, H. Luo, W. Fu, K. Furukawa, Activation of NF- κ B protects hippocampal neurons against oxidative stress-induced apoptosis: evidence for induction of manganese superoxide dismutase and suppression of peroxynitrite production and protein tyrosine nitration, *J. Neurosci. Res.* 49 (1997) 681–697, [https://doi.org/10.1002/\(SICI\)1097-4547\(19970915\)49:6<681::AID-JNR3>3.0.CO;2-3](https://doi.org/10.1002/(SICI)1097-4547(19970915)49:6<681::AID-JNR3>3.0.CO;2-3).
- [41] E. Weaver, C. O'Hagan, D.A. Lamprou, The sustainability of emerging technologies for use in pharmaceutical manufacturing, *Expert Opin. Drug Deliv.* 19 (2022) 861–872, <https://doi.org/10.1080/17425247.2022.2093857>.
- [42] N.M. Belliveau, J. Huft, P.J. Lin, S. Chen, A.K. Leung, T.J. Leaver, A.W. Wild, J. B. Lee, R.J. Taylor, Y.K. Tam, C.L. Hansen, P.R. Cullis, Microfluidic synthesis of highly potent limit-size lipid nanoparticles for in vivo delivery of siRNA, *Mol. Ther. Nucleic Acids* 1 (2012) e37, <https://doi.org/10.1038/mtna.2012.28>.
- [43] F. Sommonte, I. Arduino, R.M. Iacobazzi, L. Laera, T. Silvestri, A.A. Lopodota, A. Castegna, N. Denora, Microfluidic development of brain-derived neurotrophic factor loaded solid lipid nanoparticles: an in vitro evaluation in the post-traumatic brain injury neuroinflammation model, *J. Drug Deliv. Sci. Technol.* 96 (2024) 105699, <https://doi.org/10.1016/j.jddst.2024.105699>.
- [44] P. Mantuano, B. Boccanegra, E. Conte, M. De Bellis, S. Cirri, F. Sanarica, O. Cappellari, I. Arduino, A. Cutrignelli, A.A. Lopodota, A. Mele, N. Denora, A. De Luca, β -Dystroglycan Restoration and Pathology progression in the Dystrophic mdx mouse: Outcome and implication of a clinically Oriented study with a Novel oral Dasatinib formulation, *Biomolecules* 11 (2021) 1742, <https://doi.org/10.3390/biom11111742>.
- [45] G. Graverini, V. Piazzini, E. Landucci, D. Pantano, P. Nardiello, F. Casamenti, D. E. Pellegrini-Giampietro, A.R. Bilia, M.C. Bergonzi, Solid lipid nanoparticles for delivery of andrographolide across the blood-brain barrier: in vitro and in vivo evaluation, *Colloids Surf. B Biointerfaces* 161 (2018) 302–313, <https://doi.org/10.1016/j.colsurfb.2017.10.062>.
- [46] L. Gastaldi, L. Battaglia, E. Peira, D. Chirio, E. Muntoni, I. Solazzi, M. Gallarate, F. Dosio, Solid lipid nanoparticles as vehicles of drugs to the brain: Current state of the art, *Eur. J. Pharm. Biopharm.* 87 (2014) 433–444, <https://doi.org/10.1016/j.ejpb.2014.05.004>.
- [47] F. Lupoli, T. Vannocci, G. Longo, N. Niccolai, A. Pastore, The role of oxidative stress in Friedreich's ataxia, *FEBS Lett.* 592 (2018) 718–727, <https://doi.org/10.1002/1873-3468.12928>.
- [48] C.M.T. Marobbio, I. Pisano, V. Porcelli, F.M. Lasorsa, L. Palmieri, Rapamycin reduces oxidative stress in frataxin-deficient yeast cells, *Mitochondrion* 12 (2012) 156–161, <https://doi.org/10.1016/j.mito.2011.07.001>.
- [49] B. Kalyanaraman, V. Darley-Usmar, K.J.A. Davies, P.A. Dennery, H.J. Forman, M. B. Grisham, G.E. Mann, K. Moore, L.J. Roberts, H. Ischiropoulos, Measuring reactive oxygen and nitrogen species with fluorescent probes: challenges and limitations, *Free Radic. Biol. Med.* 52 (2012) 1–6, <https://doi.org/10.1016/j.freeradbiomed.2011.09.030>.
- [50] R.J. Mark, J.N. Keller, I. Kruman, M.P. Mattson, Basic FGF attenuates amyloid β -peptide-induced oxidative stress, mitochondrial dysfunction, and impairment of Na⁺/K⁺-ATPase activity in hippocampal neurons, *Brain Res.* 756 (1997) 205–214, [https://doi.org/10.1016/S0006-8993\(97\)00196-0](https://doi.org/10.1016/S0006-8993(97)00196-0).
- [51] P. González-Cabo, F. Palau, Mitochondrial pathophysiology in Friedreich's ataxia, *J. Neurochem.* 126 (2013) 53–64, <https://doi.org/10.1111/jnc.12303>.
- [52] H. Puccio, D. Simon, M. Cossée, P. Criqui-Filipe, F. Tiziano, J. Melki, C. Hindelang, R. Matyas, P. Rustin, M. Koenig, Mouse models for Friedreich ataxia exhibit cardiomyopathy, sensory nerve defect and Fe-S enzyme deficiency followed by intramitochondrial iron deposits, *Nat. Genet.* 27 (2001) 181–186, <https://doi.org/10.1038/84818>.
- [53] M. Whitnall, Y.S. Rahmanto, M.L.-H. Huang, F. Saletta, H.C. Lok, L. Gutiérrez, F. J. Lázaro, A.J. Fleming, T.G. St Pierre, M.R. Mikhael, P. Ponka, D.R. Richardson, Identification of nonferritin mitochondrial iron deposits in a mouse model of Friedreich ataxia, *Proc. Natl. Acad. Sci. USA* 109 (2012) 20590–20595, <https://doi.org/10.1073/pnas.1215349109>.